Unconventional beam amplification with photovoltaic and diffusion effects in a He^+-implanted $LiNbO_3$:Fe waveguide

Alexandre Dazzi, Pierre Mathey, Pierre Lompré, and Pierre Jullien

Laboratoire de Physique de l'Université de Bourgogne, Matériaux pour l'Optique Non Linéaire, Unité Propre de Recherche 5027, Enseignement Supérieur Associée, Centre National de la Recherche Scientifique, 9 Avenue Alain Savary, B.P. 400, 21011 Dijon Cedex, France

Serguey G. Odoulov

Institute of Physics, National Academy of Sciences, 46 Science Avenue, 252 650 Kiev-22, Ukraine

Paul Moretti

Laboratoire de Physico Chimie des Matériaux Luminescents, Unité Mixte de Recherche 5620, Centre National de la Recherche Scientifique, Université Claude Bernard Lyon 1, 43 Boulevard du 11 Novembre 1918, 69622 Villeurbanne, France

Received June 29, 1998

Two-wave mixing at 514.5 nm is investigated in an x-cut $LiNbO_3$:Fe waveguide twice implanted with helium ions. The energy transfer is studied in four configurations characterized by the orientation of the optical axis and the polarization of the input waves. It is shown that, in one arrangement, the kinetics of the wave mixing consists of two parts: a transient peak attributed to the photovoltaic effect followed by a slower decay toward the stationary state for which the classic diffusion mechanism is predominant. The appearance of the photovoltaic effect is unexpected in comparison with the results found for the bulk. © 1999 Optical Society of America [S0740-3224(99)00102-2]

OCIS codes: 160.5320, 190.7070, 130.2790, 040.5350, 130.3730.

1. INTRODUCTION

Nonlinear interactions in optical waveguides offer many promising applications such as second-harmonic generation obtained, for example, in Ti-diffused $LiNbO_3$ waveguides,[1] in periodically poled Ti:$LiNbO_3$,[2] and in ion-implanted $KNbO_3$ planar guides,[3] photorefractive amplification, and phase conjugation. The possibility of a photoinduced change in the refractive index permits the recording of holograms in waveguides. This characteristic can be exploited for holographic amplification of light beams. For the last application, the main interest of the integrated devices lies in the fact that high power density is easily achieved. Inasmuch as the response time of the photorefractive phenomenon is inversely proportional to the intensity, shorter response times can be reached in the guide than in the bulk. This possibility has been demonstrated for in materials such as H^+-implanted $BaTiO_3$.[4] In most earlier studies, the self-diffraction of light in planar optical waveguides has been investigated.[5–7] Fewer studies have treated wave amplification through the photorefractive effect in proton- or He-implanted strontium barium niobate[8] ($Sr_{0.61}Ba_{0.39}Nb_2O_6$) or in proton-exchanged $LiTaO_3$.[9] Generally, the wave coupling is attributed to diffusion or photovoltaic mechanisms. These properties, combined with the those of mode confinement, successfully explain the recording of holograms in planar $LiNbO_3$ waveguides.[7] The previous studies conducted with $LiNbO_3$ have dealt with waveguides fabricated with Ti or Fe indiffusion or by the proton-exchange process. In the present study we investigate two-beam coupling in a He-implanted waveguide fabricated with an Fe-doped $LiNbO_3$. In Section 2 we characterize the waveguide optically. Two-wave mixing is investigated in Section 3; in particular, we show that the temporal behavior of the energy transfer consists of a transient peak followed by a decrease toward the steady state. Experimental investigations to elucidate the origin of the transient energy transfer are described. Transient and steady-state gains are studied relative to the intensity ratio of the incident waves. A discussion follows in Section 4. We recall that an oscillatory character in the kinetics of two-wave mixing has been already observed in bulk materials and in waveguides made by diffusion. We show that, in our guide, the magnitudes of the photovoltaic and diffusion electric fields are of the same order, which explains the shape of the temporal behavior of the two-wave mixing.

2. WAVEGUIDE FABRICATION AND CHARACTERIZATION

Our planar waveguide is fabricated from an x-cut $LiNbO_3$:Fe substrate (0.01-wt. % Fe) whose dimensions

are 2 mm × 10 mm × 12 mm, with the 10-mm edges along the *c* axis and the 2-mm edges along the *x* axis. All the faces of the guide are optically polished. The optical barrier is generated with two successive He^+-ion implantations at energies of 2 and 1.9 MeV, each at a dose of 1×10^{16} ions/cm^2. This double He implantation creates a sufficiently thick optical barrier and high step index to minimize energy leaks through it.[10]

The waveguiding properties of the sample are investigated with a classic *m*-lines arrangement. The good quality of the guiding shows that no postimplantation repolishing or annealing is necessary, unlike for H^+-implanted waveguides. TE or TM modes are selectively injected into the waveguide by extraordinarily or ordinarily polarized light ($\lambda = 514.5$ nm) propagating parallel or perpendicular to the *c* direction. The corresponding *m*-lines spectra are shown in Fig. 1. Sharp and well-contrasted dark lines are observed for each polarization and whatever the direction of propagation is (parallel or perpendicular to the optical axis). From the angular positions of the dark lines, the effective indices are calculated and exploited to reconstruct the corresponding index profiles.[11] These calculations indicate that the guide depth is approximately 5 μm, the optical barrier thickness is ~0.5 μm, and the extraordinary and the ordinary step indices are, respectively, $\Delta n_e \approx 7 \times 10^{-3}$ and $\Delta n_o \approx 8 \times 10^{-2}$.

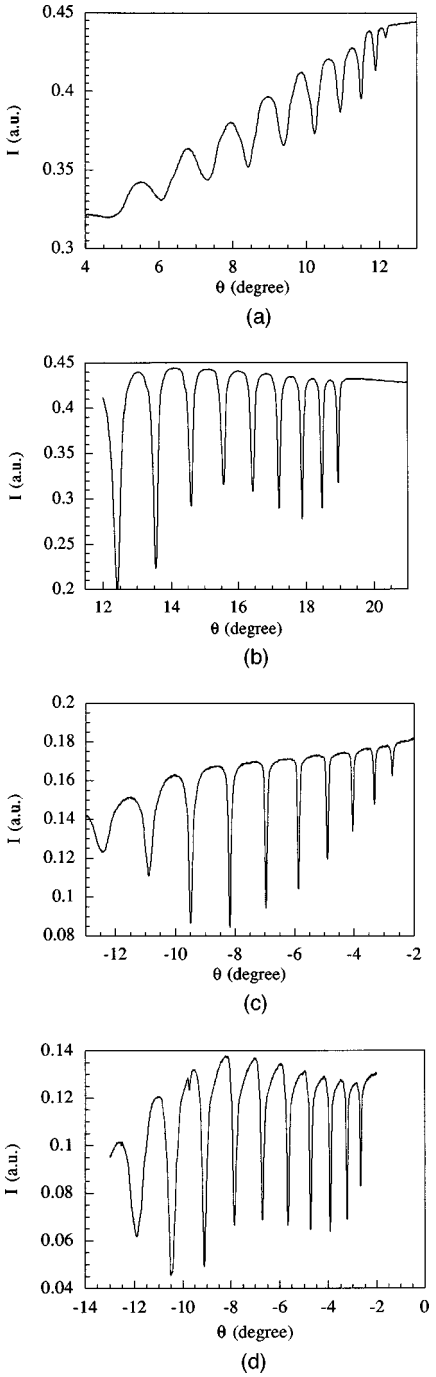

Fig. 1. *m*-Lines spectra at 514.5 nm in an x-cut $LiNbO_3$:Fe waveguide for propagation of (a) TE-polarized light perpendicular to the *c* axis, (b) TE-polarized light along the *c* axis, (c) TM-polarized light perpendicular to the *c* axis, and (d) TM-polarized light along the *c* axis.

Using the same arrangement as that described in a previous paper by some of the present authors,[10] we analyze the modal structure of the guided light. The analysis reveals that, whatever the sample orientation and the polarization of the input light are, the outcoupled light has two orthogonal TE and TM components, in accordance with the theoretical propagation properties in anisotropic waveguides.[12,13]

3. WAVE MIXING

Two incident beams issued from an Ar-ion laser are injected into the waveguiding layer with a rutile input prism. The use of input prisms offers the advantage of selective coupling of a mode with a given and well-defined order, avoids the possibility of multimode injection, and minimizes the interaction of the two beams as would happen in an arrangement involving microscope objectives. The two waves travel at an angle $\pm\theta = 7°$ inside the guide with the interaction length of 1 mm. The weak input beam is the probe; the strongest one is the pump. Both beams are outcoupled with another rutile prism. Four configurations that depend on the orientation of the optical axis and the input polarization are investigated (see Fig. 2).

A. Guiding Properties

The coupling efficiencies of the second guided mode deduced from the magnitude of the dark line in the *m*-lines spectra are 2%, 25%, 33%, and 9% for the configurations in Figs. 2(a), 2(b), 2(c), and 2(d), respectively. In these four configurations the waves inside the guide are elliptically polarized. The output anisotropic prism divides them into TE and TM beams. For the configuration of Fig. 2(a) the intensity ratio on the probe beam is ~0.1 and on the pump beam is ~0.3. For the three other configurations the intensity ratio is $\sim 10^{-2}$. In what follows, the input intensities of the beams are adjusted at sufficiently low levels to prevent their self-focusing or self-defocusing.[14,15] With these intensities we did not observe temporal evolution of the spatial structure of the emerging beams after 10 min. Consequently the observed energy transfers between the beams are not affected by this phenomenon. Moreover, between succes-

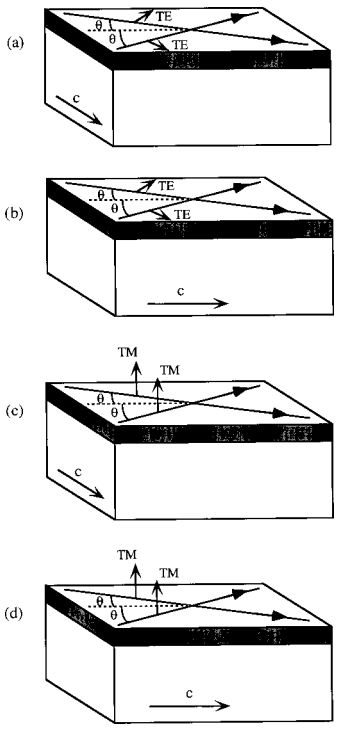

Fig. 2. Schematic representations of the beams, their polarizations, and their relative dispositions with respect to the optical axis.

sive measurements we take care to erase with uniform illumination all the gratings previously recorded in the material.

B. Beam Coupling

In a first step, we investigate the two-beam coupling with the experimental configuration depicted in Fig. 2(a) for which two TE_1 modes are injected with a coupling efficiency of 2%. A typical set of kinetic curves for the four outcoupled light beams (TE_1 and TM_1 on the pump and probe arms) is plotted in Fig. 3. The simultaneous amplification of the TE_1 and TM_1 components on the probe beam and the corresponding depletion of the TE_1 and TM_1 pump beams are systematically observed for several ratios r of the pump–probe intensities. This ratio is measured on the TE_1 outcoupled beams. The temporal behavior of the probe beam begins with a rather fast rise of the signal, followed by a slower decay toward a steady state. Note (see Fig. 3) that each TM component faithfully follows the corresponding TE beam, so we believe that there is no TE_1–TM_1 energy transfer. The transient energy peak indicated by the arrow in Fig. 3(a) in the signal is attributed to the photovoltaic effect (see the discussion in Section 4 for more details). To reinforce this interpretation we verified that the peak occurs even when the pump and the probe are interchanged (see Fig. 4), with the orientation of the c axis retained.[16,17] Thus the associated energy transfer is unidirectional: It always amplifies the weak beam at the expense of the pump, and the reversal of the polar axis does not alter the direction of the energy exchange.[18,19] Moreover, a monotonic temporal rise of the probe when the ratio r is equal to unity is obtained. All these observations tend to prove that, in the first instant after the pump is switched on, the amplification of the probe comes mainly from the photovoltaic effect. The second part of the kinetic curves, i.e., the slow decay to the steady state, is essentially due to the classic diffusion phenomenon because the associated energy transfer becomes opposite when the pump and probe beams are interchanged.[20] This fact is illustrated in Fig. 4, where the intensity level of the stationary state is below the initial probe intensity.

Two response times, τ_p and τ_s, are defined to characterize the kinetics. The first (τ_p) is relative to the transient peak, and τ_s corresponds to the part of the curve

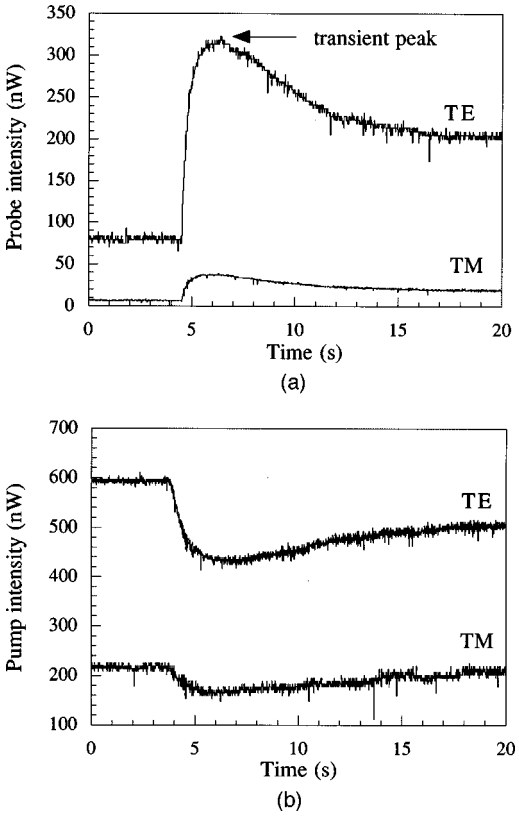

Fig. 3. Typical kinetic curves of (a) the amplification of the TE and TM components of the probe, (b) the depletion of the TE and TM components of the pump. For these curves we take $r \approx 9$; the total estimated intensity inside the guide is 3.9 W/cm^2. The configuration corresponds to that in Fig. 2(a).

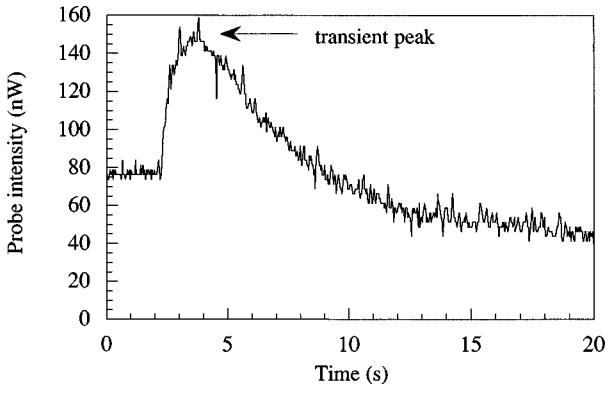

Fig. 4. Kinetic curve of the TE outcoupled probe beam obtained by interchanging of the probe and pump beams from those in the arrangement used in Fig. 3.

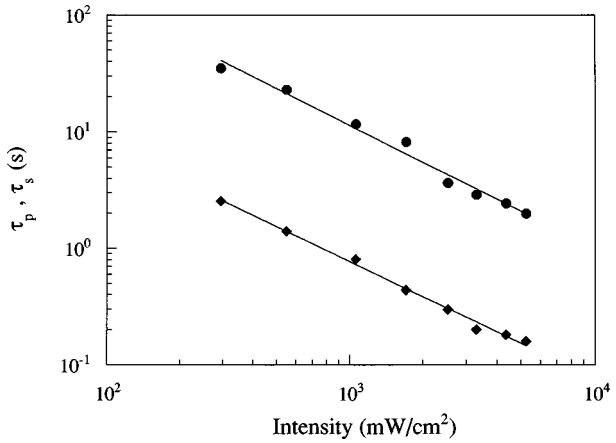

Fig. 5. Intensity dependence of the response times τ_p (filled squares) and τ_s (filled circles). Straight lines, fits of the experimental data with sublinear functions. The ratio r is fixed at $r \approx 9$.

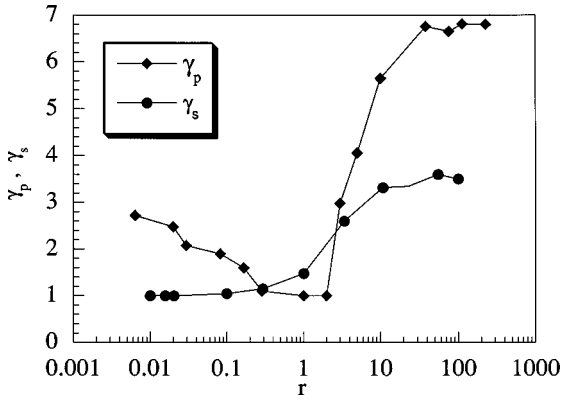

Fig. 6. Amplification factors γ_p and γ_s versus ratio r. The total incident intensity is kept constant (3.2 W/cm^2).

that is decreasing to the steady state. We obtain each time constant by fitting the appropriate ranges of the TE_1 probe beam's kinetic curve with single exponentional laws. For a given ratio $r = 9$ the intensity dependences of τ_p and τ_s are plotted in Fig. 5. The two straight lines in Fig. 5 are numerical fits of the experimental data to an I^{-x} form and illustrate the linear dependence of the response times on the total incident intensity. The exponents are close to 1 for the photovoltaic and diffusion constant times. The linear behavior of τ_s is in agreement with the fact that only one center has to be taken into account at low intensity levels ($\leqslant 10^3$ mW/cm^2) in $LiNbO_3$:Fe.[21,22] We fixed the total incident intensity at $I = 3.2$ mW/cm^2 and investigated the amplification factors γ_p and γ_s relative to the transient peak and to the stationary state. These factors are defined as

$$\gamma_p = \frac{\text{Probe intensity at the transient peak value}}{\text{Probe intensity when the pump is off}}, \tag{1}$$

$$\gamma_s = \frac{\text{Probe intensity at steady state}}{\text{Probe intensity when the pump is off}}. \tag{2}$$

The results, plotted in Fig. 6, exhibit the different behaviors of the amplification factors relative to ratio r and consequently confirm the different physical mechanisms from which they originate. The amplification factor γ_s increases monotically from values $\gamma_s \approx 1$ to a saturation, $\gamma_s \approx 3.5$. It must be noticed that γ_s increases significantly if r takes values greater than unity. All these properties are typical of an amplification whose main contribution comes from a diffusion mechanism. The shape of amplification γ_p is different. It shows that whatever ratio r is (less or greater than unity), amplification γ_p exists and so does not depend on the positions of the pump and the probe beams relative to the direction of the c axis. It also proves that there is no transient energy exchange associated with the local nonlinear mechanism.[19] As r increases and takes values close to 1, γ_p continuously decreases to weak values ($\gamma_p \approx 1$) and then increases toward a flat saturation ($\gamma_p \approx 7$). This behavior is significant for the predominant part of a photovoltaic effect.

If TM modes are injected (ordinarily polarized waves), two configurations are studied, as represented in Figs. 2(c) and 2(d). Once again, two TE and TM modes are observed on each outcoupled pump and probe beam. The results with the configuration of Fig. 2(c) are the following: The time evolution of the probe beam is a monotonic increase that tends to a steady state; no transient peak is detected as in the configuration of Fig. 2(a). The energy transfer depends on the beam disposition with respect to the c axis. The variations of γ_s as well as its directional feature are in accordance with an amplification process generated by the diffusion mechanism. The dependence of γ_s on ratio r is similar to that described in the configuration of Fig. 2(a), and the maximum amplification is $\gamma_s \approx 1.6$, obtained for ratios greater than 10.

No beam amplification for any ratio r or for any mode number is detected with the configurations of Figs. 2(b) and 2(d), unlike for the theoretical predictions that take into account the effective electro-optic coefficient in the bulk. Other experimental results underline the difference between the bulk and the waveguide: For equal power densities we are able to erase with uniform illumination a recorded grating written in the waveguide even though the recorded hologram in the bulk is fixed.

4. DISCUSSION

The photovoltaic effect in ferroelectric crystals is one of the mechanisms, with the diffusion process and the drift in an external electric field, that are used to record holograms. In $LiNbO_3$ and $LiTaO_3$ crystals, photovoltaic fields as high as 10^4–10^5 V/cm can be generated.[16] The feasibility of Hologram writing in $LiNbO_3$ planar waveguides has been demonstrated experimentally by several authors. The amplification of a weak beam regardless of the directions of the recording beams with respect to the optical axis has been demonstrated in an experimental situation[23] that was similar to that in the present study. In the research reported in Ref. 23, two TE modes are injected into y-cut Ti indiffused $LiNbO_3$:Fe whose optical axis lies in the incident plane, and the guided waves propagate in the xz plane. The temporal oscillatory behavior that occurs in the gain or in the diffraction efficiency has been analyzed and attributed to the photovoltaic mechanism. Note that the influence of this phenomenon and its role on the temporal grating buildup

have also been investigated for pure or Fe-doped $LiNbO_3$ and $LiTaO_3$ crystals.[24–26] In all these studies it has been demonstrated that (1) the oscillatory character of the energy redistribution originates from a transient phase mismatch of the recorded phase grating and fringe pattern when the interacting beams have different intensities, (2) for equal light intensities, the kinetics are smooth, and the gain coincides with the usual stationary gain that is due to diffusion, (3) the energy is always transferred to the weak beam [see Eqs. (7) and (8) of Ref. 25]. We emphasize that the transient peak described in Section 3 obeys each of the three above points. In the publications mentioned above it was also stated that the additional nonshifted volume phase grating, which is responsible for the oscillations, may come from an external applied electric field or can be internal like the photovoltaic field. Let us recall that, under an electric field E_0, the expression for the stationary space-charge field is[20]

$$E_{sc} = \frac{(E_0^2 + E_D^2)^{1/2}}{\left[\left(1 + \frac{E_D}{E_q}\right)^2 + \left(\frac{E_0}{E_q}\right)^2\right]^{1/2}}, \tag{3}$$

where E_D is the diffusion field and E_q is the saturation field.

The temporal law for the space-charge field is given by

$$E_1(t) = mE_{sc}[1 - \exp(-t/\tau)], \tag{4}$$

with

$$\frac{1}{\tau} = \frac{1}{\tau_{DI}}\left(\frac{K_{diff}}{K_{Debye}}\right)^2 \times \frac{(K^2 + K_{Debye}^2)(K^2 + K_{diff}^2) + \left(KE_0\frac{e}{k_BT}\right)^2}{(K^2 + K_{diff}^2)^2 + \left(KE_0\frac{e}{k_BT}\right)^2} + \frac{1}{j\tau_{DI}}\left(\frac{K_{diff}}{K_{Debye}}\right)^2 \frac{(K^2 - K_{Debye}^2)\left(KE_0\frac{e}{k_BT}\right)}{(K^2 + K_{diff}^2)^2 + \left(KE_0\frac{e}{k_BT}\right)^2}, \tag{5}$$

where $K_{diff} = K\sqrt{\tau_D/\tau_R}$ is the inverse of the diffusion length, $K_{Debye} = K[(\tau_I\tau_D)/(\tau_R\tau_{DI})]^{1/2}$ is the Debye screening length, τ_D is the diffusion constant time, τ_R is the recombination time constant, τ_{DI} is the dielectric relaxation time, and K is the grating vector.

The point to underline is that in when $E_0 = 0$, i.e., for no external applied electric field or for no photovoltaic effect, the imaginary part of τ vanishes and so the oscillatory feature disappears. This result is in accordance with our experimental observations made with the configuration of Fig. 2(a) and for $r = 1$.

To estimate the magnitude of the field $E_0 = E_{pv}$ that originates from the photovoltaic effect, we write that, under open-circuit conditions, the photovoltaic current density is

$$j = \sigma E_{pv} = \kappa\alpha I, \tag{6}$$

where σ is the photoconductivity (the dark conductivity is negligible at our intensities), κ is the photovoltaic coefficient, α is the absorption, and I is the light intensity. For our waveguide the photoconductivity $\sigma \approx 4 \times 10^{-11}\ \Omega^{-1}\ cm^{-1}$ is deduced from the erasing kinetics curve recorded in Fig. 2(c). We take $\kappa = 2.5 \times 10^{-11}\ A\ mW^{-1}$ (Ref. 16) and $\alpha \approx 2\ cm^{-1}$; the light intensity in the guide is typically $\sim 1\ W/cm^2$. These values lead to $E_{pv} = 0.1 \times 10^5$ V/m, which is of the same order as that the space-charge field $E_{sc} = 1.9 \times 10^5$ V/m. Consequently the photovoltaic field must not be neglected, and it seems reasonable to attribute the transient energy transfer described in Section 3 to this effect. The absence of other oscillations may be the result of the short interaction length of the guided waves ($\approx$1 mm), as suggested in Ref. 6. Nevertheless, as $LiNbO_3$ belongs to the $3m$ class, the only coefficient of the antisymmetric part of the photovoltaic tensor is β_{131}^a, so the photovoltaic current density should vanish along the optical axis. Consequently, no photovoltaic contribution to the energy transfer should be observed. The breaking of the symmetry as a result of the implantation process or because of special properties that arise from the light confinement in the waveguiding layer could be some explanations for this.

5. CONCLUSION

The energy transfer in an x-cut $LiNbO_3$:Fe waveguide fabricated by two He implantations has been investigated for the first time to our knowledge. If two TE-polarized waves propagating nearly perpendicularly to the optical axis are injected, an unexpected transient energy exchange is evidenced, independently of the orientation of the input waves with respect to the c axis. Its characteristics as well as the estimation of the photovoltaic electric field lead us to conclude that it may originate from the photovoltaic effect. Bulk $LiNbO_3$ doped with Fe is usually used to record holograms because of its high diffraction efficiencies. Here we have demonstrated that the wave mixing process in a waveguide geometry is different from that in the bulk. The energy transfer in the guide leads to amplification and opens the door to other applications.

P. Mathey's e-mail address is pmathey@u-bourgogne.fr.

REFERENCES

1. W. Sohler and H. Suche, "Second-harmonic generation in Ti-diffused $LiNbO_3$ optical waveguides with 25% conversion efficiency," Appl. Phys. Lett. **33**, 518–520 (1978).
2. J. Amin, V. Pruneri, J. Webjörn, P. St. J. Russell, D. C. Hanna, and J. S. Wilkinson, "Blue light generation in a periodically poled Ti:$LiNbO_3$ channel waveguide," Opt. Commun. **135**, 41–44 (1997).
3. T. Pliska, F. Mayer, D. Fluck, P. Günter, and D. Rytz, "Nonlinear optical investigation of the optical homogeneity of $KNbO_3$ bulk crystals and ion-implanted waveguides," J. Opt. Soc. Am. B **12**, 1878–1887 (1995).
4. K. E. Youden, S. W. James, R. W. Eason, P. J. Chandler, L. Zhang, and P. D. Townsend, "Photorefractive planar waveguides in $BaTiO_3$ fabricated by ion-beam implantation," Opt. Lett. **17**, 1509–1511 (1992).
5. O. V. Kandidova, V. V. Lemanov, and B. V. Sukharev, "Ho-

logram storage in planar lithium niobate waveguides," Sov. Tech. Phys. Lett. **9**, 335–336 (1982).
6. O. V. Kandidova, V. V. Lemanov, and B. V. Sukharev, "Self-diffraction of light in lithium niobate waveguides," Sov. Phys. Tech. Phys. **29**, 1019–1022 (1984).
7. D. Kip, F. Rickermann, and E. Krätzig, "Photorefractive recording by a special mechanism in planar $LiNbO_3$ waveguides," Opt. Lett. **20**, 1139–1141 (1995).
8. D. Kip, B. Kemper, I. Nee, R. Pankrath, and P. Moretti, "Photorefractive properties of ion-implanted waveguides in strontium barium niobate crystals," Appl. Phys. B **65**, 511–516 (1997).
9. S. M. Kostritskii, D. Kip, and E. Krätzig, "Improvement of photorefractive properties of proton-exchanged $LiTaO_3$ waveguides," Appl. Phys. B **65**, 517–522 (1997).
10. A. Dazzi, P. Mathey, and P. Jullien, "Energy leaks through the optical barrier created by H^+ implantation in $BaTiO_3$ and $LiNbO_3$ waveguides," Opt. Commun. **149**, 135–142 (1998).
11. P. Mathey, P. Jullien, and J. L. Bolzinger, "Refractive-index profile reconstructions in planar waveguides by the WKB inverse method and reflectivity calculations," J. Opt. Soc. Am. B **12**, 1663–1670 (1995).
12. D. Marcuse, "Modes of a symmetric slab optical waveguide in birefringent media. II. Slab with coplanar optical axis," IEEE J. Quantum Electron. **QE-15**, 92–101 (1979).
13. M. Lu and M. M. Fejer, "Anisotropic dielectric waveguides," J. Opt. Soc. Am. B **10**, 246–261 (1993).
14. A. Ashkin, G. D. Boyd, J. M. Dziedzic, R. G. Smith, A. A. Ballman, J. J. Levinstein, and K. Nassau, "Optically-induced refractive index inhomogeneities in $LiNbO_3$ and $LiTaO_3$," Appl. Phys. Lett. **9**, 72–74 (1966).
15. Q. W. Song, C. Zhang, and P. J. Talbot, "Self-defocusing, self-focusing, and speckle in $LiNbO_3$ and $LiNbO_3$:Fe crystals," Appl. Opt. **32**, 7266–7271 (1993).
16. A. M. Glass, D. von der Linde, and T. J. Negran, "High-voltage bulk photovoltaic effect and the photorefractive process in $LiNbO_3$," Appl. Phys. Lett. **25**, 233–235 (1974).
17. S. G. Odoulov, "Spatially oscillating photovoltaic current in iron-doped lithium niobate crystals," JETP Lett. **35**, 10–13 (1982).
18. B. I. Sturman, "The photogalvanic effect—a mechanism of non linear wave interaction in electrooptic crystals," Sov. J. Quantum Electron. **10**, 276–278 (1980).
19. S. G. Odoulov and B. I. Sturman, "Four-wave polarization interaction in photorefractive crystals," Sov. Phys. JETP **65**, 1134–1144 (1987).
20. P. Günter and J.-P. Huignard, *Photorefractive Materials and Their Applications* (Springer-Verlag, Heidelberg, 1988, 1989), Vols. I and II.
21. E. Krätzig and R. Sommerfeld, "Influence of dopants on photorefractive properties of $LiNbO_3$ crystals," in *Nonlinear Optical Materials III*, P. Günter, ed., Proc. SPIE **1273**, 58–60 (1990).
22. F. Jermann and J. Otten, "Light-induced charge transport in $LiNbO_3$:Fe at high light intensities," J. Opt. Soc. Am. B **10**, 2085–2092 (1993).
23. O. V. Kandidova, V. V. Lemanov, and B. V. Sukharev, "Hologram writing in lithium niobate planar lightguides," Sov. Phys. Tech. Phys. **9**, 335–336 (1983).
24. K. Shvarts, A. Ozols, P. Augustov, and M. Reinfelde, "Photorefraction and self enhancement of holograms in $LiNbO_3$ and $LiTaO_3$ crystals," Ferroelectrics **75**, 231–249 (1987).
25. N. Kukhtarev, V. Markov, and S. Odoulov, "Transient energy transfer during hologram formation in $LiNbO_3$ in external electric field," Opt. Commun. **23**, 338–343 (1977).
26. M. Carrascosa, J. M. Cabrera, and F. Agullo-Lopez, "Role of the photovoltaic drift on the initial writing and erasure rates of holographic gratings: some implications," Opt. Commun. **69**, 83–86 (1988).